ELSEVIER

Contents lists available at ScienceDirect

# **Applied Clay Science**

journal homepage: www.elsevier.com/locate/clay



# Research Paper



# Clay-bacteria interaction: Effect of bacterial cell density on sedimentation behavior and fabric map of kaolinite clay

Hyun-Woo Joo<sup>a</sup>, Tae-Hyuk Kwon<sup>a,\*</sup>, Sheng Dai<sup>b</sup>

- a Department of Civil and Environmental Engineering, Korea Advanced Institute of Science and Technology, Daejeon 34141, Republic of Korea
- <sup>b</sup> School of Civil and Environmental Engineering, Georgia Institute of Technology, Atlanta, GA 30332, United States

#### ARTICLE INFO

Keywords:
Kaolinite
Shewanella oneidensis MR-1
Clay-bacteria interaction
Sedimentation
Surface charge
Clay fabric

#### ABSTRACT

Clay-bacteria interactions are ubiquitous and the presence of bacteria has a pronounced effect on the mechanical, chemical, and electrical behaviors of clays. However, the role of microscale clay-bacteria interactions to the macro-scale engineering behaviors and properties of clays remains poorly understood. This study presents changes in the microstructure of kaolinite in association with bacteria and the resulting sedimentation behavior of bacterium-associated kaolin suspensions. Sedimentation tests were performed using suspensions composed of kaolin and model bacteria *Shewanella oneidensis* MR-1 while varying the fluid pH and cell density. The results reveal that kaolinite presents face-to-face aggregated microstructures with the presence of bacteria, attributable to sharing and/or exchange of cations between kaolinite and bacterial cells. Meanwhile, at a pH value lower than the isoelectric point of the kaolinite edge surfaces, the clay-bacteria association appears less pronounced comparing to the higher pH, owing to the competition between negative (kaolinite faces and bacteria surfaces) over positive (kaolinite edges) charges. The fabric change caused by kaolinite-bacteria association accelerates kaolin settling and reduces the final void ratios. A fabric map for bacterium-associated kaolinite is suggested based on the sedimentation behaviors and scanning electron microscopy observations. This study advances the understanding of particle-level clay-bacteria interactions and the sedimentation behavior of clays in suspensions with vigorous microbial activities.

# 1. Introduction

Clay sediments in freshwater as well as in marine environments contain microorganisms and biomasses such as bacteria, archaea, viruses, biominerals, and biofilms, with which they form physical and chemical interactions (Gadd, 2010; Dong, 2012; Hassard et al., 2016). Clay minerals facilitate the growth of microorganisms by supplying nutrients, providing habitat, and protecting from external stress, but at the same time, can also inhibit the growth of microorganisms by interrupting transmembrane movement that reduces respiration (Lavie and Stotzky, 1986; Wilson and Butterfield, 2014; Hassard et al., 2016; McMahon et al., 2016; Li et al., 2019). In return, microorganisms affect clay mineral formation and transformation through adsorption, metal reduction, nucleation, biofilm formation, and biomineralization (Naimark et al., 2009; Zhou et al., 2016). Those interactions have been widely used in geo-environmental practices (Zhou and Keeling, 2013; Li et al., 2019), such as wastewater treatment (Pan et al., 2006; Chen et al., 2011; Pachepsky and Shelton, 2011; Chen et al., 2018; Li et al., 2019)

and sediment remediation by removing embedded pathogenic organisms (Danovaro et al., 2008; Hassard et al., 2016) or radioactive pollutants (Perdrial et al., 2009).

Interactions between clay particles and pore fluids have a pronounced effect on clay fabric though their extent differs with clay mineralogy and pore fluid chemistry (Palomino and Santamarina, 2005). In particular, dominant interparticle forces, including van der Waals attraction and electrical force, determines the clay fabric when the confining stress is low. Moreover, the clay fabric can be affected by physical compaction in association with stress and structural anisotropy (Abu-Hassanein et al., 1996; Hasan et al., 2018). Meanwhile, bacterial cells and clay particles share common characteristics, attributable to their comparable particle size and surface charge density (Revil et al., 2012), and hence, bacterial cells coagulate with clays and affect clay fabric. Furthermore, biomasses such as cell bodies, biofilms, extracellular biopolymers, and DNA molecules also aggregate with clays in a similar way to clay-clay interaction (Alimova et al., 2009; Kwon et al., 2017; Castro-Smirnov et al., 2020).

E-mail address: t.kwon@kaist.ac.kr (T.-H. Kwon).

<sup>\*</sup> Corresponding author.

However, controversy exists regarding the interaction between clay and biomass. Some studies suggest that the electrostatic forces plays a key role in the clay-biomass interaction and ensuing adsorption of biomasses, including bacterial cells, biopolymers, and biofilms (e.g., Omoike and Chorover, 2006; Hong et al., 2011; Jia et al., 2011; Zhang et al., 2015; Kwon et al., 2017; Biswas et al., 2017; Qu et al., 2017; Su et al., 2019). By contrast, other literature argues that the physical interaction, such as physical trapping, governs the clay-biomass interaction (e.g., Pan et al., 2006; Zou et al., 2006; Castro-Smirnov et al., 2020; Kim and Kwon, 2022). Accordingly, the clay-bacterium interaction and it association mechanism at the particle level are poorly understood, and there has been limited study on its effect on sedimentation, particle aggregation, and fabric in clay sediments.

Therefore, this study explores the sedimentation behavior of claybacteria mixed suspension and the fabric of bacterium-associated clay sediments with an emphasis on clay-bacteria interaction. Kaolin is used as a model clay, and Shewanella oneidensis MR-1, which is widely used in bioremediation practices (Xiong et al., 2006; Icopini et al., 2009; Lee et al., 2018), is selected as a model bacterium. A series of sedimentation test is conducted with clay-bacteria mixed suspensions in different pH conditions and varying cell densities. Further analyses using the zeta potential and methylene blue (MB) adsorption allow examining the kaolinite-bacteria interactions and ensued effects on sedimentation behavior. Finally, this study presents a fabric map of bacteriumassociated kaolinite clay by capturing the clay-bacteria interaction, which is expected to be useful to predict the deposited volume and fabric of clay sediments under biotic environments with thriving microbial activities. The presented results advance understanding of clay-bacteria interactions under various pH conditions, and their effects on clay fabrics and engineering behaviors of bacterium-associated clay sediments.

#### 2. Materials and methods

#### 2.1. Materials

This study chose a kaolinite-dominant clay (or kaolin) as a model clay (Belitung Island Kaolin, P.T. Surya Wiraldo, Jakarta, Indonesia; Fig. 1a). The X-ray diffraction (XRD) analysis showed that the kaolin was composed of 86.5% of kaolinite and 13.5% muscovite/illite (Fig. S1a in Supporting Information; X'PERT MPD, Philips, Amsterdam, Netherlands). The model kaolin has a specific surface area of 31.2  $\text{m}^2/\text{g}$ , as measured by the MB adsorption method (Santamarina et al., 2002b), and a mean grain size of 2.26  $\mu\text{m}$ , as determined by the laser diffraction analysis (HELOS/KR, Sympatec GmbH, Clausthal-Zellerfeld, Germany). Table 1 shows the physical and index properties of the model kaolin used in this study.

Shewanella oneidensis MR-1 (ATCC# 700550), a species commonly

**Table 1**Physical and index properties of the model kaolin.

| Property                | Value   | Method/reference                          |  |
|-------------------------|---------|---|--|
| Plastic limit (%)       | 43      | Atterberg limits test                     |  |
| Liquid limit (%)        | 60      |   |  |
| Plasticity index        | 17      | PI = LL - PL                              |  |
| Specific surface area   | 0.1     | MB absorption method / Santamarina et al. |  |
| $(m^2/g)$               | 31      | (2002b)                                   |  |
| Isoelectric point (IEP) | 6.5–6.8 | Zeta potential measurement / (Pecini and  |  |
| of edge                 | 0.5-0.8 | Avena (2013); Fig. S1b)                   |  |
| D <sub>90</sub> (μm)    | 2.37    |   |  |
| $D_{50}$ (µm)           | 2.26    | Laser diffraction analysis                |  |
| $D_{10}$ (µm)           | 2.15    |   |  |

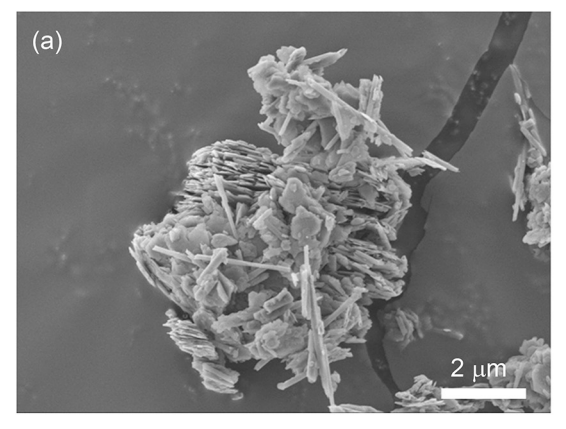
found in natural subsurface and aquatic environments, is used as the model bacterium. *S. oneidensis* MR-1 is a rod-shaped, gram-negative bacterium that can thrive under both aerobic and anaerobic conditions, as shown in Fig. 1b. It secretes biofilms and electrically conductive nanowires, allowing electrons and nutrients to be shared between bacterial cells and supporting survival under extreme conditions (Gorby et al., 2006; Ray et al., 2010; Roy et al., 2013).

#### 2.2. Solution chemical compositions

Kaolinite is a clay mineral with a platy structure composed of a 1:1 combination of silica tetrahedral and alumina dioctahedral sheets. There are three types of kaolinite surfaces, an dioctahedron surface (or O-face), a tetrahedron surface (or T-face), and an edge face. Among those surfaces, the T-face carries a permanent negative charge owing to an isomorphic substitution of Si<sup>4+</sup> by Al<sup>3+</sup>, while the O-face and edge face carry a pH-dependent charge associated with protonation, deprotonation, and cation complexation (Brady and Walther, 1989; Wieland and Stumm, 1992; Palomino and Santamarina, 2005; Tombácz and Szekeres, 2006; Tournassat et al., 2015; Zhang et al., 2022).

Accordingly, the polarity of those O-face and edge surfaces differs with pH, and the isoelectric point (IEP) is defined as the pH when electrophoretic mobility reaches zero or the pH that renders zero net charges on those surfaces (Parks, 1967; Santamarina et al., 2002a). The net surface charge of the O-face and edge surface stay negative when pH exceeds the IEP, and becomes positive once pH is lower than the IEP. The IEP of the kaolinite edge surface is reported as  $\sim$ 6.5–7 (e.g., 6.5 as reported by Kumar et al., 2017; 7.2 by Williams and Williams, 1978), and it was measured as  $\sim$ 6.5–6.8 in this study based on the variation in the zeta potential with pH (Pecini and Avena, 2013; Table 1 and see Fig. S1b). The IEP of the kaolinite O-face is approximately 4 or <4 (Williams and Williams, 1978).

Three different pH solutions were used to investigate the effect of pH on the kaolin sedimentation: above, near and below the edge IEP,



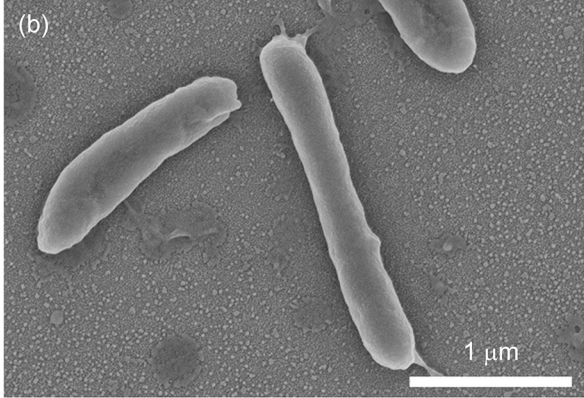


Fig. 1. Scanning electron microscope (SEM) images of (a) air-dried kaolin and (b) Shewanella oneidensis MR-1 cells attached on a glass plate. The cells were prepared through cell fixation and dehydration, as reported by Cen et al. (2004). Both samples were coated with osmium.

respectively (pH 9.1, 7.2, and 5.4, respectively). To prevent pH change due to the addition of kaolin and bacterial cells, the potassium phosphate buffers (assay  $\geq 98\%$ ; Sigma Aldrich, St. Louis, MO, USA) were used to control the pH at 5.4 and 7.2, and the sodium carbonate/bicarbonate buffer (assay  $\geq 99\%$ ; Sigma Aldrich, St. Louis, MO, USA) for pH 9.1. These pH solutions had a relatively low ionic concentration ( $\sim 0.01$  M or 450–500 ppm), which minimized the effect of salts on clay fabric formation (Palomino and Santamarina, 2005). Still, this ionic concentration was high enough to protect cell membranes against osmosis. The final salinity of the solutions was adjusted by using sodium chloride (assay  $\geq 99\%$ ; Sigma Aldrich, St. Louis, MO, USA) in addition to pH buffers. The chemical compositions of the solutions is shown in Table 2.

#### 2.3. Sample preparation and sedimentation test

Fig. 2 depicts the sample preparation process for the sedimentation test of a kaolin-bacteria mixture. A frozen stock of S. oneidensis MR-1 was resuscitated in a tryptic soy broth (TSB) medium buffered to pH 6.8 (Table 3) and cultured at 28 °C without shaking under an aerobic condition. After 48 h of growth, the cultured sample was transferred to a fresh TSB medium at a volume ratio of 1:10, and cultured again for 48 h. Then, the bacterial cells were separated from soluble extracellular polymeric substances (EPS) by centrifuging 100 mL of the bacterial culture at 13,500g under 4 °C for 15 min (first centrifugation). The supernatant separated from the bacterial cell suspension was discarded, and the remaining bacterial cells were resuspended in the same volume of an autoclaved pH solution (pH 9.1, 7.2, or 5.4). This centrifugation process was repeated two more times to thoroughly remove the remaining soluble EPS and growth media. The cell density of the buffered cell suspension was  $\sim 10^9$  cells/mL.

The buffered cell suspension was then diluted with a pure pH solution at the volume ratios of 60:0, 12:48, 1.2:58.8, 0.12:59.88, and 0.012:59.988, so as to vary the bacterial cell density in these bacterial solutions. These corresponded to the concentrations of 0.02, 0.2, 2, 20, and 100%, respectively, and hence the final cell density in the diluted bacterial solutions ranged over four orders of magnitude, i.e.,  $\sim 10^5 - 10^9$ cells/mL. The final volume of the diluted bacterial solutions was 60 mL. Finally, 3 g of oven-dried kaolin was added to 60 mL of the prepared bacterial solutions. In addition, the abiotic baseline solution was prepared by mixing 3 g of oven-dried kaolin with 60 mL of a pure pH solution. A total of six suspensions were prepared, one abiotic suspension and five kaolin-bacteria mixed suspensions. These solutions were stirred for 48 h at room temperature (~24  $^{\circ}\text{C})$  and then 10 mL of each suspension was sampled for zeta potential ( $\zeta$ ) measurements. A sedimentation test commenced by placing the remaining 50 mL of each suspension in a graduated glass cylinder. The graduated cylinder had an inner diameter of 21 mm, greater than the yield diameter, which ensured no or minimal wall effect (Michaels and Bolger, 1962). The height of the interface between the supernatant and the kaolin sediment was monitored for >48 h, as shown in Fig. 3. In this study, the initial clay concentration of the suspensions was 50 g/L, equivalent to the water content of  $\sim$ 2000% (defined as the mass ratio of water to solid). At such

**Table 2** Chemical compositions of the pH solutions.

| Compound                                   | Composition of pH solutions                             |   |  |  |
|--|---|---|--|--|
|  | pH 5.4  | pH 7.2  | pH 9.1   |  |
| NaCl                                       | 1 mM  | 1 mM  | 1 mM   |  |
| pH buffer                                  | $\mathrm{KH_2PO_4}$ 9.20 mM $\mathrm{K_2HPO_4}$ 0.80 mM | $ m KH_2PO_4~4.10$ $ m mM$ $ m K_2HPO_4~5.90$ $ m mM$ | NaHCO <sub>3</sub> 9.10<br>mM<br>Na <sub>2</sub> CO <sub>3</sub> 0.90 mM |  |
| Conductivity at 24 °C<br>Salinity at 24 °C | 1.2 mS/cm<br>499 ppm                                    | 1.0 mS/cm<br>469 ppm                                  | 1.0 mS/cm<br>469 ppm   |  |

a clay concentration, sedimentation exhibits a zone settling behavior for kaolin, in which interparticle interactions, such as the electrical force and van der Waals attraction as well as the gravimetric force, govern the coagulation and sedimentation of kaolinite (Imai, 1980). Each sedimentation test was repeated twice to confirm reproducibility.

#### 2.4. Zeta potential and cell density

The zeta potential of a kaolin-bacteria mixed suspension indicates the surface charge characteristics based on the electrophoretic mobility in the suspension according to the Smoluchowski equation (Pashley, 1985). Accordingly, the zeta potentials of the tested suspensions was measured at 25  $^{\circ}\text{C}$  before the start of the sedimentation tests by using the zeta potential analyzer (Litesizer 500, Anton Paar GmbH, Graz, Austria). Each measurement was performed with 450  $\mu\text{L}$  of a suspension and the average value of three replicates was calculated for each suspension.

The bacterial cell density in a kaolin-bacteria mixed suspension prior to the sedimentation test was measured by using the quantitative polymerase chain reaction (qPCR) analysis. The qPCR analysis counts the extracted DNA chains in a solution sample, which enabled the determination of the initial cell density in each suspension. Moreover, the cell density in the supernatant of the sedimentation column was also measured with the qPCR method at the end of the test. For the cell density, the average value of three replicates was used.

#### 2.5. Neutralization of surface charge by methylene blue (MB) adsorption

It is hypothesized that the main interaction between clay particles and bacterial cells which determines clay fabric and thus clay sedimentation behavior is the electrical force between surface charges and the van der Waals attraction (Derjaguin and Landau, 1941; Verwey, 1947; van Olphen, 1964; Derjaguin et al., 1987; Chorom and Rengasamy, 1995; Missana and Adell, 2000; Santamarina et al., 2002a). Accordingly, this study hypothesized that electrically neutralizing the surface charges of kaolinite would reduce its electrical interactions with bacterial cells during kaolin sedimentation. Therefore, to prove this hypothesis, a series of additional sedimentation tests were conducted using electrically neutralized kaolin by methylene (MB) adsorption.

In this study, MB was exploited to neutralize the negative charges on kaolinite surfaces. MB,  $C_{16}H_{18}ClN_3S$ , releases a cation  $C_{16}H_{18}N_3S^+$  in the aqueous phase that can be readily adsorbed on negatively charged surfaces of kaolinite, neutralizing the negative surface charges and dying the material blue. This feature of MB has been used to measure the specific surface area of clay minerals (Hang and Brindley, 1970; Chen et al., 1999; Santamarina et al., 2002b). Non-treated kaolin suspensions had zeta potentials of -38.2~mV at pH 9.1, -36.6~mV at pH 7.2, and - 18.6 mV at pH 5.4, respectively. The MB adsorption caused a significant increase in the zeta potentials of kaolin suspensions to -0.7, -2.4, and + 4.1 mV, respectively. This indicated that most of the negative surface charges were neutralized through MB adsorption.

As supplementary experiments, additional sedimentation tests were carried out with the MB-absorbed kaolin. The wet specific surface area of the kaolin ( $S_s = 31 \text{ m}^2/\text{g}$ ) indicates that 0.0133 g MB powder would fully coat the total surface area of 1 g kaolin. Accordingly, 0.016 g of MB per 1 g kaolin was used, *i.e.*, 1.2 times greater concentration to ensure full saturation of MB on the kaolinite surfaces. To neutralize the surface charges on the kaolinite minerals by MB adsorption, 3 g of oven-dried kaolin and 0.048 g of MB powder were mixed with 40 mL pH solution and stirred for 48 h. The buffered cell suspension of 20 mL with varying cell density from ~10<sup>5</sup> to ~10<sup>9</sup> cells/mL was then added. After stirring again for 24 h, the sedimentation tests with the mixed suspensions of MB-adsorbed kaolin and bacterial cells were commenced. The initial clay concentration of these suspensions was 50 g/L, the same as previously discussed sedimentation tests. The tests were repeated twice at pH 9.1.

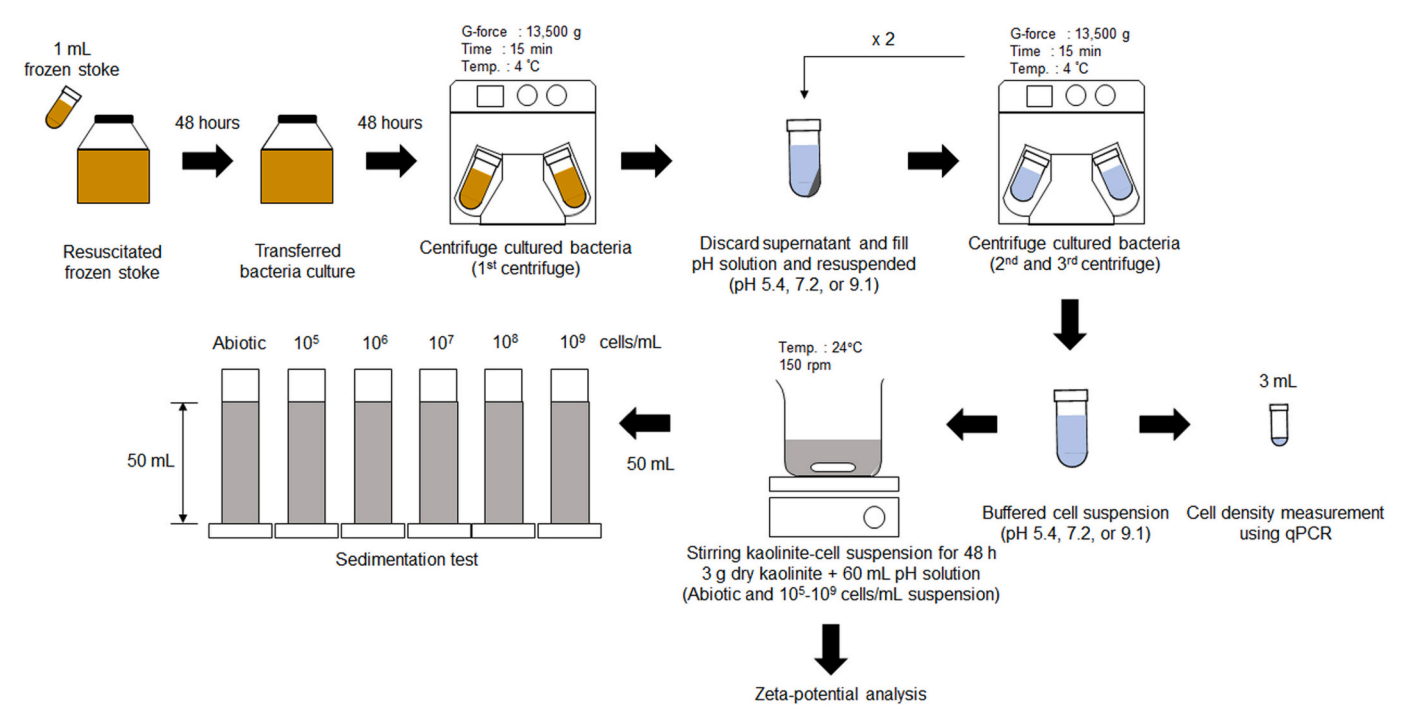


Fig. 2. A schematic diagram of the preparation of kaolin-bacteria mixed suspensions and sedimentation test.

**Table 3**Composition of the tryptic soy broth (TSB) growth medium.

| Concentration |
|---------------|
| 17 g/L        |
| 3 g/L         |
| 2.5 g/L       |
| 2.5 g/L       |
| 5 g/L         |
| 0.1 M         |
|               |

## 2.6. Optical microscopy and scanning electron microscopy (SEM) imaging

After sedimentation tests, kaolin sediment was sampled at the midpoint of the settled sediment and observed under optical and SEM microscopes for its microstructure. For optical microscopic imaging, the sampled sediment was diluted to 3% to prevent particle and/or floc overlap, and it was then injected into a microfluidic chip, composed of polydimethylsiloxane (PDMS) with a 25  $\mu m$  height and 50  $\mu m$  width channel. The kaolinite-bacterial cell ratio and pore fluid chemistry were kept consistent with that in the sedimentation tests. The sampled sediment for SEM imaging was immediately stored in a - 80 °C freezer and dried using a freeze dryer (FreeZone, Labconoco Corporation, Kansas City, Missouri, USA) to minimize fabric change during the drying process (Aiyama et al., 2019). The dried samples were then coated with osmium and used for SEM imaging.

# 3. Results

#### 3.1. Abiotic sedimentation – effects of pH

As illustrated in Fig. 4a (Michaels and Bolger, 1962; Imai, 1980; Imai, 1981), clay suspension sedimentation typically involves three stages. In *the flocculation stage*, clay particles do not settle much but mainly make flocs due to interparticle forces. Subsequently, flocs of clay particles start to settle, which is called *the settling stage*, and the downward movement of the interface between the supernatant and the settling suspension shows almost a constant velocity, referred as the

settling rate. Eventually, the interface settling slows down compared to that at the settling stage and enters into *the consolidation stage*, in which the settled flocs start to physically interact with each other *via* self-weight consolidation. The settling rate and the final void ratio of the sediment were reported to describe the sedimentation behavior of kaolin in this study.

The sedimentation behavior of kaolin is strongly affected by pH and this pH dependency is more pronounced in a low salinity condition with low ionic strength (Palomino and Santamarina, 2005). Fig. 4b shows the sedimentation curves at three different pH conditions with 0.01 M salinity, similar to surface water conditions. The tests were repeated four times and averaged. All tests exhibited a liquid-like sedimentation behavior. The fastest sedimentation occured at pH 7.2 with a settling rate of 10.5 cm/h, followed by 9.56 cm/h at pH 5.4, and the slowest settling rate of 1.23 cm/h at pH 9.1.

When the pH exceeds the IEP of the kaolinite edge, owing to the negatively charged kaolinite edge and face surfaces, the electrical repulsion dominates particle-to-particle interactions. This produces a mixed fabric composed of dispersed and face-to-face aggregation (FF aggregation) due to the cation adsorption on the kaolinite face at pH 9.1 and 0.01 M salinity (Palomino and Santamarina, 2005). Accordingly, our results indicate that the high degree of repulsion and the mixed fabric at pH 9.1 led to the slowest settling rate (1.23 cm/h) and the longest time taken to converge to the final void ratio ( $\sim$ 48 h), as shown in Fig. 4b.

At pH 7.2, close to the IEP of the kaolinite edge, edge-to-edge flocculation (EE flocculation) becomes the dominant fabric due to van der Waals attraction between edges that are electrically neutralized. The highly flocculated structure with a low level of electrical repulsion at pH 7.2 induced approximately 10 times faster sedimentation (10.5 cm/h) than that at pH 9.1. In addition, it was particularly seen that the supernatant at pH 7.2 was cloudy due to non-associated suspended fines.

The sedimentation at pH 5.4, which is much less than the IEP of the kaolinite edge, generates an edge-to-face flocculation (EF flocculation) due to the electrical attraction between negatively charged faces and positively charged edges. This pH condition also produces a highly flocculated fabric. Accordingly, the sedimentation was fast (9.56 cm/h) and quickly reached the final void ratio, similar to the result at pH 7.2

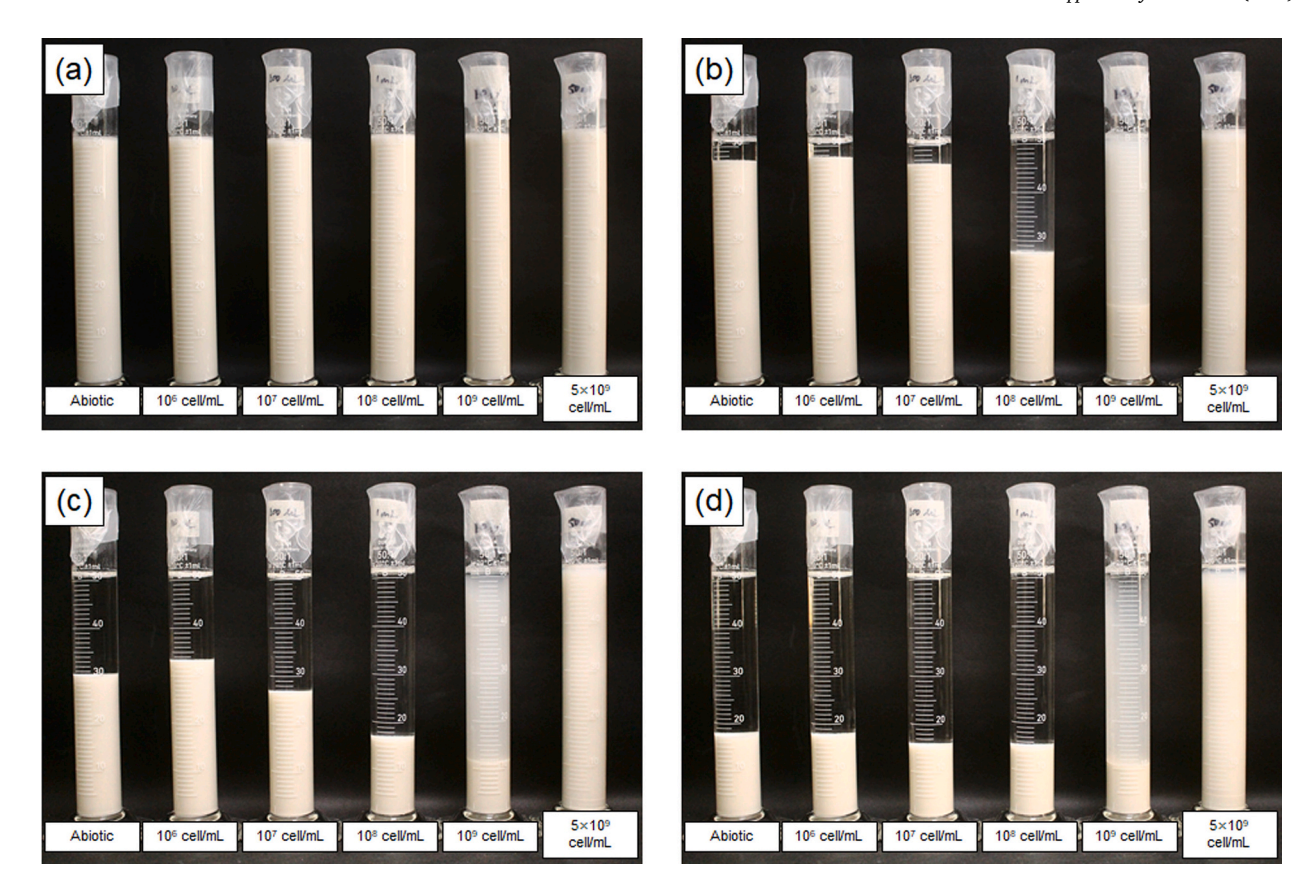


**Fig. 3.** Time-lapse photographs of the kaolin-bacteria suspension sedimentation tests. The photos show the sedimentation behaviors under pH 9.1 at the elapsed times: (a) t = 0, (b) t = 1, (c) t = 6, and (d) t = 24 h. From left to right, the suspension contains a cell density of 0,  $10^6$ ,  $10^7$ ,  $10^8$ ,  $10^9$ , or  $5 \times 10^9$  cells/mL.

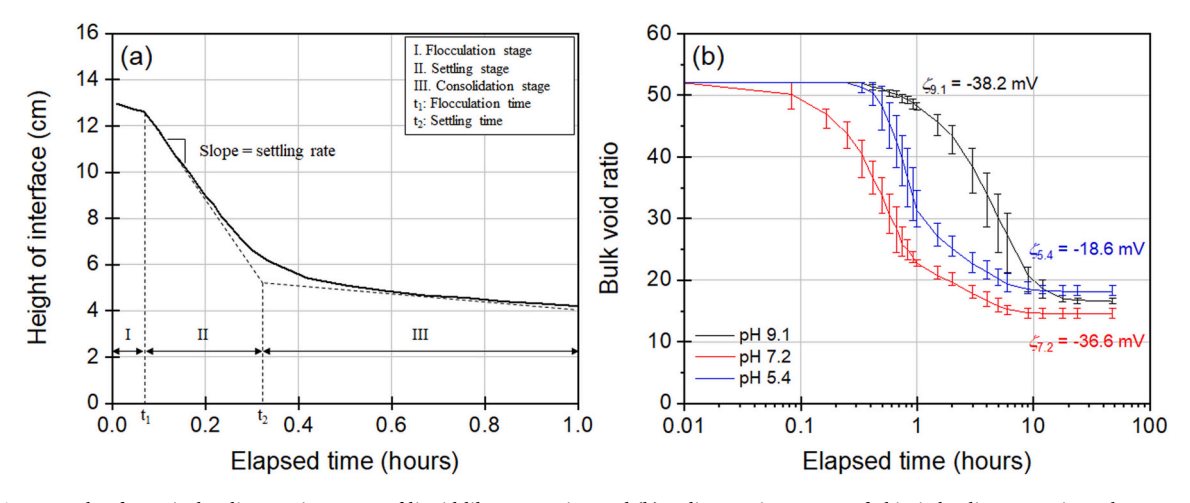


Fig. 4. (a) An example of a typical sedimentation curve of liquid-like suspension and (b) sedimentation curves of abiotic kaolin suspension. The curves in (b) were plotted by averaging the results from four repeated tests, and the error bars denote the maximum and minimum values.

(Fig. 4b). It was interestingly noted that the sedimentation column at pH 5.4 had a clear supernatant, while it showed a longer flocculation time than at pH 7.1, almost as long as that at pH 9.1. The EF flocculated structure at pH 5.4 resulted in the highest final void ratio among the three pH conditions. These observations from the abiotic kaolin sedimentation tests are well consistent with previous study results reported by Palomino and Santamarina (2005).

# 3.2. Biotic sedimentation - effects of bacterial cell density

The sedimentation test curves of bacteria-associated kaolin, which

were performed twice at each pH with varying cell densities, are shown in Fig. 5. When the cell density was  $\sim\!10^7$  cells/mL or less, there was no evident difference between biotic and abiotic sedimentation curves. However, the results clearly show that the kaolin sedimentation accelerated when the cell density exceeded  $\sim\!10^8$  cell/mL. As a comparison, the settling stage in the abiotic test lasted about 10 h, while that in the cases with the cell density  $>\!10^8$  cells/mL took only a few minutes to several tens of minutes. This trend was consistently observed for all three pH conditions.

As shown in Fig. 6, when the cell density exceeded  $10^7$  cells/mL, as the bacterial cell density increased, the final void ratio decreased

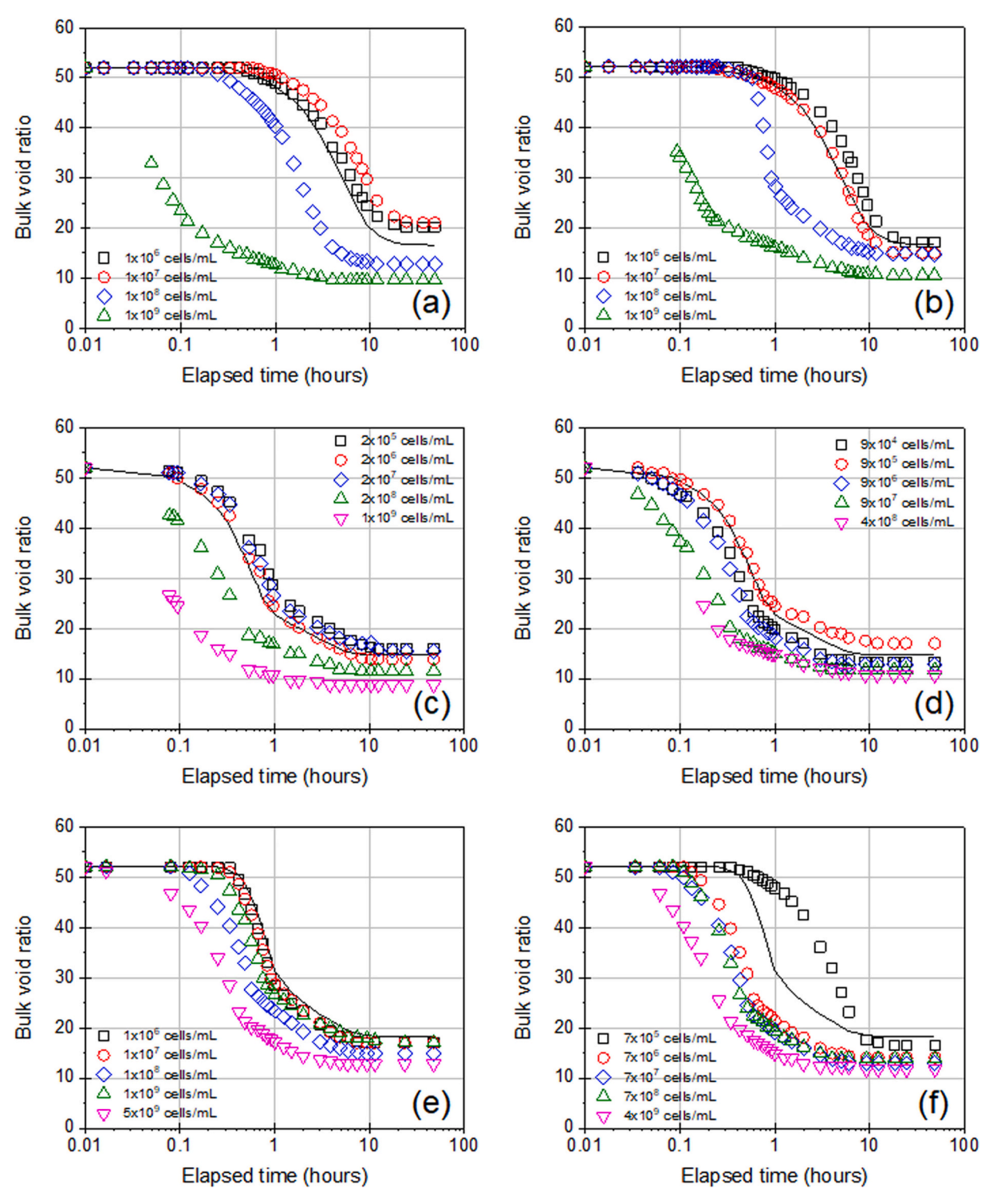


Fig. 5. Sedimentation curves of biotic bacteria-associated kaolin suspensions: (a) and (b) results at pH 9.1, (c) and (d) results at pH 7.2, and (e) and (f) results at pH 5.4. Black lines indicate the sedimentation curve of an abiotic kaolin suspension. The results with the highest cell density,  $5 \times 10^9$  cells/mL, at pH 9.1 are not included in this figure.

(Fig. 6a), the settling rate accelerated (Fig. 6b), and the equivalent hydraulic diameter became larger (Fig. 6c). When the cell density was  $<10^7$  cells/mL, the trend was not unclear.The equivalent hydraulic diameter  $D_i$  at the ith time step during settling can be estimated using Stokes' law, as follows:

$$D_i = \sqrt{\frac{18\mu}{(G_S - 1)\rho_w}} \times \sqrt{\nu_i},\tag{1}$$

where  $\mu$  is the dynamic viscosity of the fluid;  $G_S$  is the specific gravity of kaolinite; and  $\nu_i$  is the settling rate at the ith time step. The average hydraulic diameter was obtained by averaging  $D_i$  during the entire settling stage. Note that Stokes' law assumes no interparticle interactions among particles or flocs. However, the high clay concentration (50 g/L) used in this study unavoidably caused the interparticle interactions, such as electrical interaction and van der Waals attraction. Therefore, the hydraulic diameter estimated using Stokes' law was only

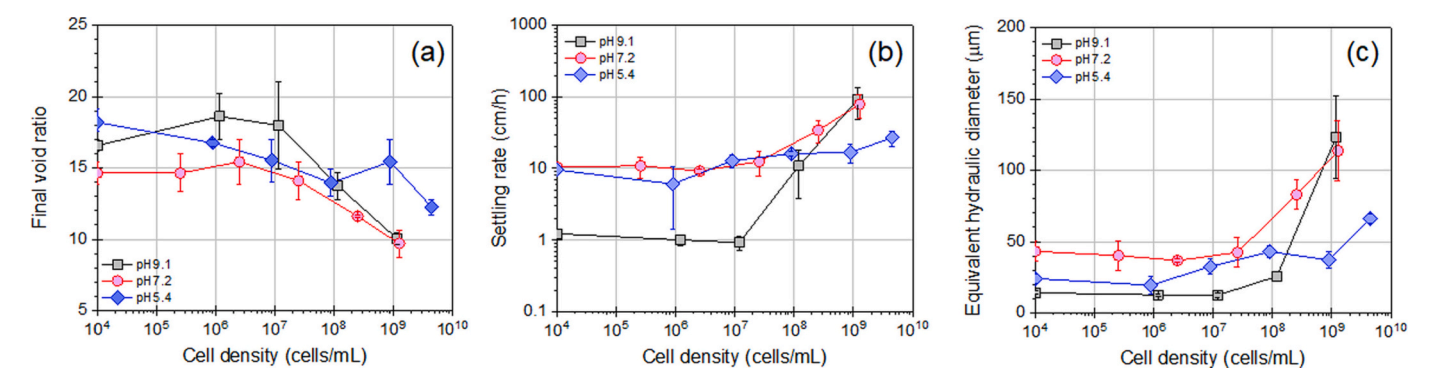


Fig. 6. Effect of cell density on sedimentation behavior: (a) final void ratio, (b) settling rate, and (c) equivalent hydraulic diameter estimated from Stokes' law. The data points at 10<sup>4</sup> cells/mL represent the abiotic test results. Each data point indicates the mean value from duplicates and the error bar indicates the range of the result.

for qualitative comparison and not to determine absolute floc sizes.

At pH 9.1, which is above the IEP of the kaolinite edge, both the face and the edge of the kaolinite surface are negatively charged, resulting in electrical repulsion between the kaolinite and *S. oneidensis* MR-1 cell surfaces. As a result of electrical repulsion (Hong et al., 2011; Jia et al., 2011) at cell densities  $<\!10^7$  cells/mL, a kaolin-bacteria suspension presented delayed sedimentation and/or a higher final void ratio compared to an abiotic kaolin suspension. For example, under pH 9.1, the final void ratio increased from 16.6 to 18.0, and the settling rate decreased from 1.23 to 0.92 cm/h at  $\sim\!10^7$  cells/mL.

On the other hand, sedimentation of the kaolin-bacteria mixture was significantly accelerated when the cell density exceeded  $10^7$  cells/mL. Under cell-rich conditions, negatively charged clay mineral and bacterial cell surfaces can aggregate by sharing cations or exchange organic cations (Yee et al., 2000; Li et al., 2019; Guo et al., 2020). In such cases, the cations reduces the electrical repulsion between negative surface charges on minerals and bacterial cells. Through aggregation with S. oneidensis cells, kaolinite formed much larger flocs, with equivalent hydraulic diameters from  $\sim\!14$  to  $\sim\!120~\mu m$ ; therefore, the settling rate increased from 1.23 to 92.3 cm/h at  $10^9$  cells/mL. It also formed a significantly denser sediment with a final void ratio of 10.0.

Additionally, when the cell density approached  $5 \times 10^9$  cells/mL, a different sedimentation behavior was observed with the formation of macro-flocs, instead of micro-flocs (Mhashhash et al., 2018). In this case, there was a bottom-up interface between the sediment and the supernatant, and the suspension had a cloudy supernatant due to non-associated fine particles. This class of sedimentation behavior is called solid-like sedimentation or accumulation sediment (Pierre et al., 1995; Ma and Pierre, 1992; Kwon et al., 2017). The sedimentation curve analysis, such as settling rate and equivalent hydraulic diameter, was not feasible for this solid-like sedimentation.

Rather than electrical interaction, van der Waals attraction governs the particle flocculation at pH 7.2, near the IEP of the kaolinite edge. Therefore, there was minimal change in the sedimentation behavior at pH 7.2 when the cell density was  $<3\times10^7$  cells/mL. Under high cell density conditions (i.e.,  $>10^8$  cells/mL), with an increase in cell density, kaolin sedimentation accelerated by cell-clay aggregation. Finally, at the cell density of  $10^9$  cells/mL, the final void ratio decreased from 14.6 to 9.71, the settling rate increased from 10.15 to 78.97 cm/h, and the equivalent hydraulic diameter became larger from  $\sim\!43$  to  $\sim\!113$   $\mu m$ . Interestingly, at the highest cell density condition of  $\sim\!10^9$  cells/mL, the final void ratio, settling rate, and hydraulic diameter at pH 9.1 and pH 7.2 were almost identical.

Finally, at pH 5.4, which is below the IEP of the kaolinite edge, same with other pH conditions, the floc size of kaolinite-cell aggregation increased, the settling rate gradually increased, and the final sediment void ratio decreased with an increase in the cell density. However, the extent of change was less than that in the other pH conditions. For

example, when the cell density was  ${\sim}10^9$  cells/mL, the equivalent hydraulic diameter at pH 5.4 increased from 24 to 66  $\mu m$ , while it increased markedly from 14 to 120  $\mu m$  at pH 9.1 and from 43 to 113  $\mu m$  at pH 7.2, respectively. This difference is mainly attributed to the positive charges on the kaolinite edge at pH 5.4, where negative charges on the kaolinite faces and bacterial cells competing for the positive charges on the kaolinite edges. Thus, the bacterial effect can easily be compensated by the kaolinite faces. This will be further discussed in Section 4.1.

#### 4. Analysis and discussion

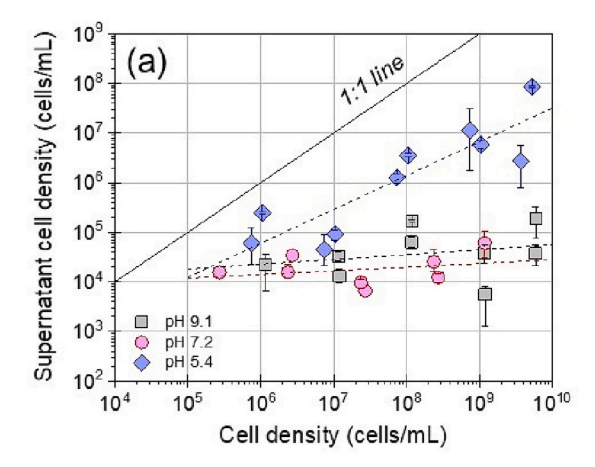
#### 4.1. The role of pH in kaolinite-cell interaction

Sedimentation test results reveal that the presence of bacteria alters kaolin sedimentation behavior at all three tested pH conditions, particularly when the cell density is  $>10^7$  cells/mL. Under such cell-rich conditions, bacterial cells share and exchange cations with kaolinite, which produces kaolinite-cell aggregation. This aggregation reduces flocculation and thus lowers the final void ratio, as shown in cases of pH 9.1 and pH 7.2 with  $10^9$  cells/mL cell density. Meanwhile, however, the aggregation produces a larger floc size and causes a faster settling rate. In addition, the results at pH 5.4 under the cell-rich condition reveal that there can be competition between bacterial cells and negatively charged kaolinite surfaces for positively charged edge surfaces, and this can suppress the effect of the presence of bacteria on kaolin sedimentation.

By contrast, in cell-poor conditions, for instance, when the cell density is  $<10^7$  cells/mL, the presence of bacteria plays different roles in kaolin sedimentation depending on pH values. At pH above the IEP of the kaolinite edge (e.g., pH 9.1), the final void ratio shows a slight increase due to electrical repulsion. At pH near the IEP of the kaolinite edge (e.g., pH 7.2), there is only minimal change. However, at pH below IEP (e.g., pH 5.4) where the kaolinite edge is positively charged, the Coulombic electrical attraction between negatively charged cell surfaces and the positively charged kaolinite edges causes a gradual decrease in the final void ratio with an increase in the cell density under the cell-poor conditions as well as the cell-rich conditions. This result is fundamentally consistent with previous studies, which have presented the electrical attraction between clay surfaces and biomaterials (Omoike and Chorover, 2006; Hong et al., 2011; Jia et al., 2011; Zhang et al., 2015).

#### 4.2. Kaolinite-cell association

The cell density remaining in supernatant after sedimentation tests indicates the density of cells un-associated with clays; therefore, it can be used to examine the degree of association between kaolinite and bacteria. The supernatant cell density after sedimentation is shown in Fig. 7a, against the initial cell density in the suspension before



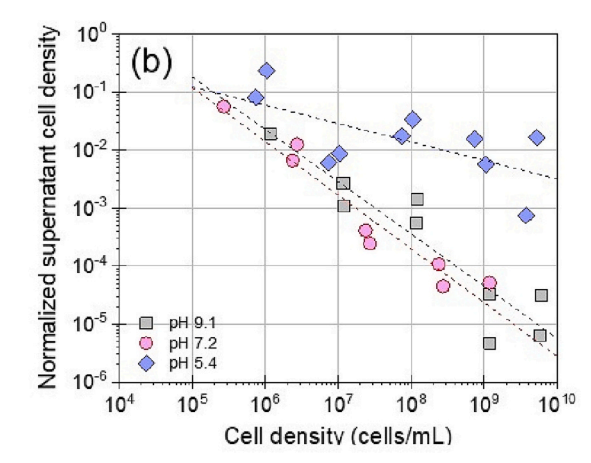


Fig. 7. Cell density in supernatants after sedimentation against the initial cell density in suspensions before sedimentation: (a) the supernatant cell density and (b) the supernatant cell density normalized with the initial cell density. All the cell density values were measured by the qPCR method.

sedimentation. At pH above and near the IEP of the kaolinite edge (pH 7.2 and 9.1), the unassociated cell density in the supernatant was consistently maintained at  $10^4$ – $10^5$  cells/mL, regardless of the initial cell density before sedimentation, as shown in Fig. 7a. However, at pH below the IEP of the kaolinite edge (pH 5.4), the un-associated cell density ranged  $10^6$ – $10^8$  cells/mL under the cell-rich conditions, which was significantly greater than that at the other pH conditions, and it increased with the initial cell density.

This trend is more clearly seen when the supernatant cell density is normalized by the initial cell density, as shown in Fig. 7b. The normalized cell density starts with 1 and it decreases with initial cell density in all pH conditions. This result clearly suggests that the cells tend to aggregate with kaolinite regardless of pH, and the extent of aggregation increases with an increase in the initial cell density. Meanwhile, the extent of aggregation is more or less the same at pH 9.1 and pH 7.2. However, at pH 5.4, the kaolinite-cell association is significantly suppressed; its un-associated cell density is 100 times greater than that at other pHs in a cell-rich condition. This result also implies the competition between negatively charged kaolinite and cell surfaces for the positively charged kaolinite edge.

The cell-to-clay particle ratio can be simply examined by assuming a disc-shaped kaolinite particle with a diameter of 2.26  $\mu m$  (i.e.,  $D_{50}$  in Table 1) and a thickness of 1/30 of its diameter. Then, there are  $\sim \! 3 \times \! 10^{12}$  kaolinite particles in 50 mL of the kaolin suspension at the clay concentration of 50 g/L. As an exemplary calculation, in the tested suspensions with the initial cell densities of  $10^6$  and  $10^9$  cells/mL, the cell-to-particle ratios were approximately  $1.6 \times 10^{-5}$ – $1.6 \times 10^{-2}$  cells per single kaolinite particle. Noting that the S. onedensis cell is  $\sim \! 1$ –3  $\mu m$  long, such low cell-to-particle ratios imply that the kaolinite particles were abundant and many were not associated with bacterial cells in this study.

# 4.3. Zeta potential of kaolinite-bacterial cell mixture

Zeta potential ( $\zeta$ ) is the potential of the shear plane in the diffuse double layer of charged particles. It is used widely to estimate the surface charge density of charged particles such as clay minerals (Williams and Williams, 1978; Yong and Ohtsubo, 1987; Syngouna and Chrysikopoulos, 2010; Tsujimoto et al., 2013). The electrical repulsive force between charged particles is proportional to the square of the zeta potential  $\zeta$ , and hence the zeta potential  $\zeta$  indirectly indicates the electrical stability of the system (Hogg et al., 1966; Scales et al., 1998; Hunter, 2001; Leong and Ong, 2003). Most clay minerals and biomaterials possess negative zeta potentials ( $\zeta$  < 0). The absolute  $\zeta$  value increases as the negative charge on the surfaces increases, and hence, the electrical repulsion increases. Conversely, a low absolute  $\zeta$  value implies low

electrical repulsion among particles, where particles readily aggregate and/or flocculate. It is reported that suspensions with negatively charged particles are highly aggregated when  $|\zeta| < 25$ . But, they are highly dispersed when  $|\zeta| > 30$  (Sapsford et al., 2011; Barhoum et al., 2018; Shnoudeh et al., 2019).

The variations in zeta potentials of the pH-buffered S. oneidensis MR-1 cell suspensions without kaolin with the cell density are shown in Fig. 8a. The measured zeta potential stayed nearly zero when the cell density was  $<10^8$  cells/mL (i.e., cell-poor conditions). But under the cell-rich conditions ( $>10^8$  cells/mL), the zeta potential evidently decreased with increased cell density. In addition, the effect of pH on the zeta potential of the cell suspensions was minimal, with the lowest zeta potentials observed at pH 7.2.

The variations in zeta potentials of kaolin-bacteria mixed suspensions with the cell density prior to sedimentation are shown in Fig. 8b. The kaolin-bacteria mixed suspensions showed the highest zeta potentials at pH 5.4 and the lowest values at pH 9.1. The  $\zeta$  values of the claycell suspensions was apparently lower than that of pure cell suspensions (Fig. 8a and b). The addition of cells to kaolin suspensions reduced the zeta potential at all pH conditions. However, this effect soon diminished when the cell density exceeded  $10^8$  cells/mL. This implies that further addition of bacterial cells hardly increases the electrical repulsion above a certain cell density. It may be because the majority of clay particles are aggregated with bacterial cells and the clay surfaces are electrically stabilized owing to abundant cell presence.

It was further explored that whether the zeta potential of clay-cell mixed suspensions before sedimentation can be an indicator of the sedimentation behavior, as shown in Fig. 8c and d. Although the trend is somewhat diffuse, it is observed that suspensions with the higher zeta potentials (or lower absolute  $\zeta$  values) result in the lower final void ratios, the faster sedimentation rates, due to less electrical repulsion and more aggregation. However, there are also outliers, which indicate the limitation of zeta potential as a good indicator of sedimentation behavior, mainly because other factors like van der Waals attraction, mechanical and structural interaction, hydrophobicity, and steric effect also play roles in inter-particle and cell-clay interactions. It is worth noting that the zeta potential only represents the electrical interaction in the system (Horie and Fujita, 2011; Shnoudeh et al., 2019), and it is not identical to the surface potential for soft materials such as biomass (Hayashi et al., 2001; Abu-Lail and Camesano, 2003).

# 4.4. Effects of kaolinite surface charge on kaolinite-cell interaction: sedimentation after MB adsorption

MB carries a positively charged molecular structure when ionized in an aqueous phase, making it readily adsorbed on negatively charged

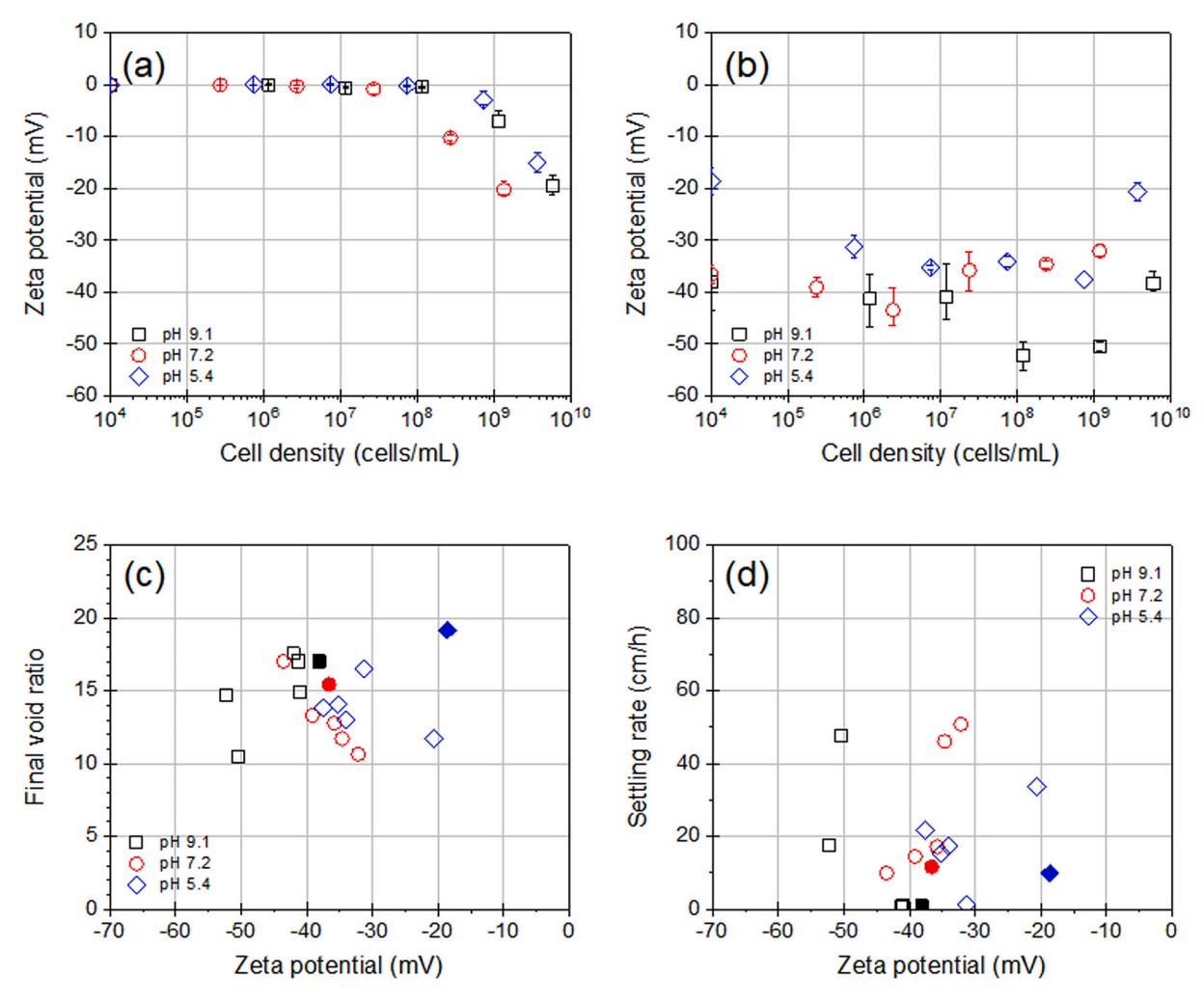


Fig. 8. Interplays among zeta potential  $\zeta$ , cell density, and sedimentation behavior: variations in (a) zeta potentials of pH-buffered cell suspensions without kaolin, and (b) zeta potentials of kaolin-bacteria mixed suspensions before sedimentation with cell density, and relations between the zeta potentials of the kaolin-bacteria suspensions and (c) the final void ratios and (d) the sedimentation rate. The solid symbols in (c) and (d) denote the abiotic results.

surfaces. Therefore, the addition of MB into kaolin suspensions lowers the absolute zeta potential close to zero, as shown in Fig. 9a. This indicates that ionized MB can electrically neutralize the kaolinite surfaces by adsorption. Upon MB adsorption, the effect of negative surface charges on kaolinite-bacteria association was investigated through sedimentation tests with the MB-adsorbed kaolin at pH 9.1.(Fig. 9).

The results indicate that under cell-poor conditions, the reduced electrical repulsion due to MB adsorption caused a decrease in final void ratio and an increase in settling rate, comparing to the non-treated kaolin suspensions, as shown in Fig. 9b and c. By contrast, under cellrich conditions, the MB adsorption showed an opposite effect, where the settling rate of MB-treated suspensions was slower and the final void ratio was lower than that of non-treated suspensions. This is because clay-cell aggregation is more pronounced in non-treated suspensions than in the MB-treated suspensions. Nevertheless, the supernatant cell density of MB-treated columns was significantly higher by 10-100 times than that of non-treated columns (Fig. 9d). The kaolinite-cell interaction greatly diminished when negative surface charges of kaolinite were neutralized. The presented result reveals that negative charges of clay surfaces plays a key role in clay-bacteria association, which accelerates the sedimentation rate, lowers the final void ratio, and stabilizes clay sediments. This can be explained with sharing of cations between cells and kaolinite particles, which compensates the repulsions between negatively charged surfaces on kaolinite and bacteria, and leads to aggregation. By contrast, when the surface charge of kaolinite is minimal,

van der Waals attraction and physical trapping become the dominant interaction between kaolinite and bacteria with weak aggregation between the two.

# 4.5. Effects of bacterial species on kaolin sedimentation

To examine the sedimentation behavior of kaolin-bacteria mixed suspensions with different bacterial species, additional tests were performed using *Leuconostoc mesenteroides*, a round gram-negative bacterium with a smaller cell size than *S. oneidensis* MR-1, as well as natural bacterial community sampled from Gapcheon in Daejeon, South Korea (Fig. S2a). Strains of the mixed bacteria culture from Gapcheon were verified using the new generation sequencing (NGS) method (Fig. S2b). The methods for bacterial cultivation and suspension preparation were identical to those for *S. oneidensis* MR-1.

The results with L. *mesenteroides* and the mixed culture show that the general observations for kaolin-bacteria sedimentation stay consistent regardless of the bacterial species, as shown in Fig. 10, which includes: (1) a minimal or decelerated effect on kaolin sedimentation under cell-poor conditions, (2) an abrupt change in sedimentation behavior at the cell density of  $10^7$ – $10^8$  cells/mL, and (3) the highest final void ratio and the slowest settling rate at pH 5.4 with a positively charged kaolinite edge. These results indicate that bacterial cell accelerates kaolin sedimentation in general, and that cell density and pH condition are more critical in kaolinite-bacteria sedimentation than the strain of bacteria.

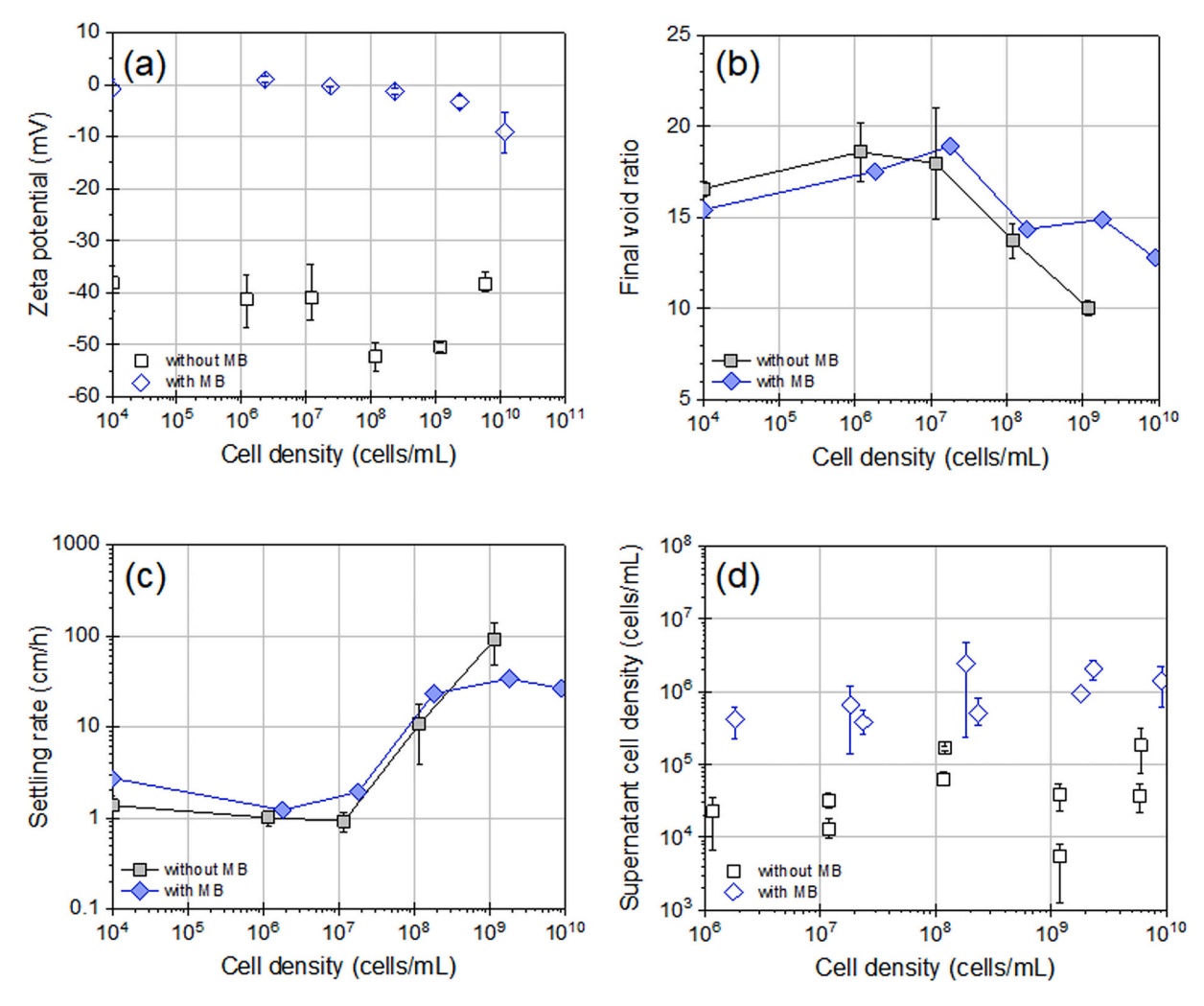


Fig. 9. Sedimentation test results of the methylene blue-adsorbed kaolin suspensions at pH 9.1: (a) the zeta potential of the kaolin-bacteria suspensions, (b) the final void ratios after sedimentation, (c) the settling rate, and (d) the cell density of supernatant after sedimentation. (For interpretation of the references to colour in this figure legend, the reader is referred to the web version of this article.)

Meanwhile, particularly at pH 7.2, it is worth noting that the cell density in the L. *mesenteroides* supernatant was >10 times greater than that in the S. oneidensis MR-1 supernatant (Figs. 7a and S3a). L. mesenteroides cells are 0.7–1.2  $\mu$ m in size (Özcan et al., 2019), which is smaller than S. oneidensis MR-1 cells which have 1.2–9.6  $\mu$ m in size (Abboud et al., 2005). At pH 7.2, the zeta potential of L. mesenteroides suspensions without kaolin was slightly lower than that of S. oneidensis MR-1 suspensions (Fig. S3b), which implies that L. meseteroides cells have a higher surface charge density than S. oneidensis MR-1 cells (Figs. 8a and S3b). Therefore, it is presumed that the the surface charge density and geometry of bacterial cells affect clay-bacteria interactions, which warrants further research.

#### 4.6. The fabric map of bacterium-associated kaolinite

Clay fabric is classified as dispersed, EE flocculation, EF flocculation, and FF aggregation (Schofield and Samson, 1954; van Olphen, 1977; Palomino and Santamarina, 2005). Palomino and Santamarina (2005) have previously presented the fabric map of kaolinite with respect to the ionic concentration and pH. In this study, the microstructure of kaolinite clay, with respect to cell density relative to 1 g kaolinite clay, is investigated through optical microscopy and SEM imaging after the sedimentation tests (Fig. 11). The optical microscopy images enable us to infer the floc size in the presence of excess water. The SEM images allow visualizing the particle-to-particle arrangement.

In the absence of bacteria, kaolinite particles at pH 9.1, above the IEP of the kaolinite edge, exhibit a dispersed fabric due to electrical repulsion. At pH 7.2 near the IEP, van der Waals attraction between neutralized edges become dominant. At pH 5.4 below the IEP, the kaolinite edge-to-face electrical attraction is prevalent. This induces a flocculated microstructure at pH 7.2 and 5.4, and additionally, kaolinite particles form some FF aggregations due to surrounding cations. This trend is consistent with the fabric map reported in Palomino and Santamarina (2005).

In the presence of bacteria, FF aggregation becomes more dominant and the floc size increases as the cell density increases regardless of pH. At pH 7.2 and 5.4, FF aggregation is more prevalent than EF/EE floculation with increased cell density. It is worth pointing out that kaolinite clay particles form macro-flocs and show a solid-like sedimentation behavior at pH greater than the IEP of the kaolinite edge (pH 9.1).

Fig. 12 depicts the fabric map of kaolinite clay in the presence of bacteria under a low salinity condition with the following three global trends. (a) The pH affects the kaolinite fabric based on its relative value to IEP: the dispersion or FF aggregation fabric becomes dominant above the IEP, and the flocculation fabric becomes dominant below the IEP. (b) When the cell density in clay-bacteria mixtures increases, FF aggregation with reduced particle-to-particle distance becomes more prevalent. And (c) FF aggregation between clay particles and bacterial cells occurs more frequently under non-positively charged edge conditions (*i.e.*, pH

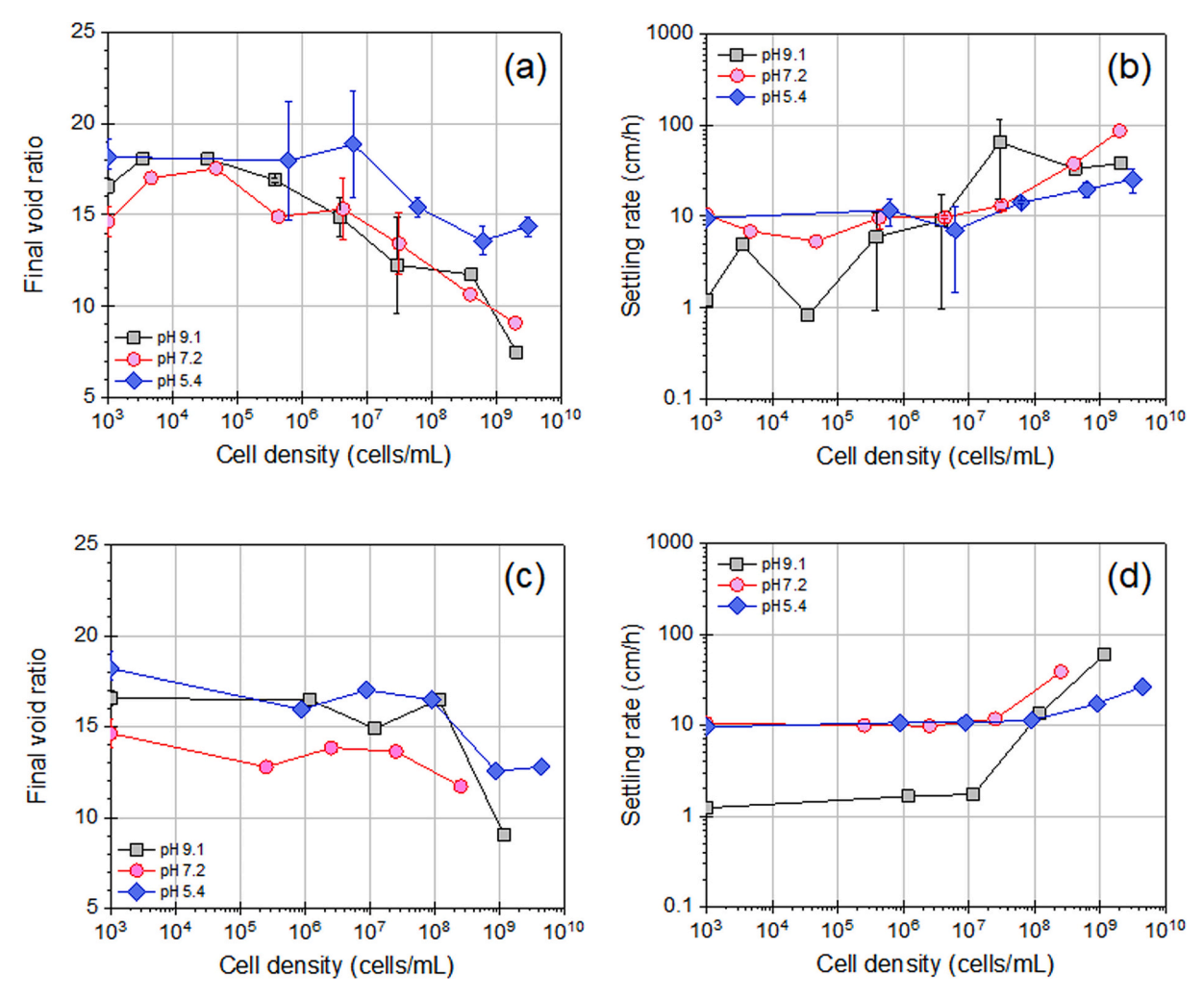


**Fig. 10.** Characterization of the sedimentation curves: (a) the final void ratio of the sediment and (b) the settling rate in the settling stage with *Leuconostoc mesenteroides*, (c) the final void ratio of the sediment and (d) the settling rate in the settling stage with mixed bacteria culture sampled in Gapcheon shown in Fig. S2. The data points at 10<sup>3</sup> cells/mL represent the abiotic test results.

> IEP). The presented fabric map allows prediction of clay fabric and sedimentation behaviors of kaolinite clay in the presence of bacteria. The fabric map provides further insight into particle-level clay-bacteria interactions and it is expected to provide a guide in engineering design for clay sediment under biotic environments with thriving microbial growth and activities.

#### 5. Conclusion

This study investigates the sedimentation behavior of kaolin-bacterial suspensions considering various pH and bacterial cell densities. The presented fabric map of kaolinite-bacteria suspensions clearly shows the pronounced effect on the sedimentation behavior and microstructure of kaolinite in biotic environments. Main findings of this study are as follows:

- If there are sufficient cations to share between negatively charged surfaces, bacterial cell accelerates kaolin sedimentation and induces lower final void ratios in the settled sediments. This is mainly due to the aggregation between kaolinite particles and bacterial cell via sharing and/or exchanging cations on their surface, and the consequent fabric change.
- The kaolinite-bacterial cell association is largely affected by pH. Kaolinite-bacteria interactions are the strongest under non-positively

- charged conditions, *i.e.*, in pH conditions that exceed or are close to the IEP of the kaolinite edge, despite the higher electrical repulsion.
- In the case of positively charged edge condition, i.e., pH is less than
  the IEP of kaolinite edge, the kaolinite-bacteria interaction is suppressed owing to the competition between the negatively charged
  kaolinite faces and bacterial cells to occupy positively charged
  kaolinite edges.
- Clay-bacteria interaction accelerates kaolin sedimentation and results in stiffer sediment in cell-rich environment. Face-to-face aggregation becomes dominant as the cell density increases. And fabric change in kaolinite due to the presence of bacteria becomes more pronounced at pH values above the IEP of the kaolinite edge.

This study advances the understanding of particle-level clay-bacteria interactions and macro-scale sedimentation behavior of clays where microbial activities are vigorous in saturated loose clay deposits.

#### CRediT authorship contribution statement

**Hyun-Woo Joo:** Methodology, Formal analysis, Validation, Investigation, Writing – original draft. **Tae-Hyuk Kwon:** Conceptualization, Methodology, Resources, Supervision, Funding acquisition, Writing – review & editing. **Sheng Dai:** Conceptualization, Methodology, Writing – review & editing.

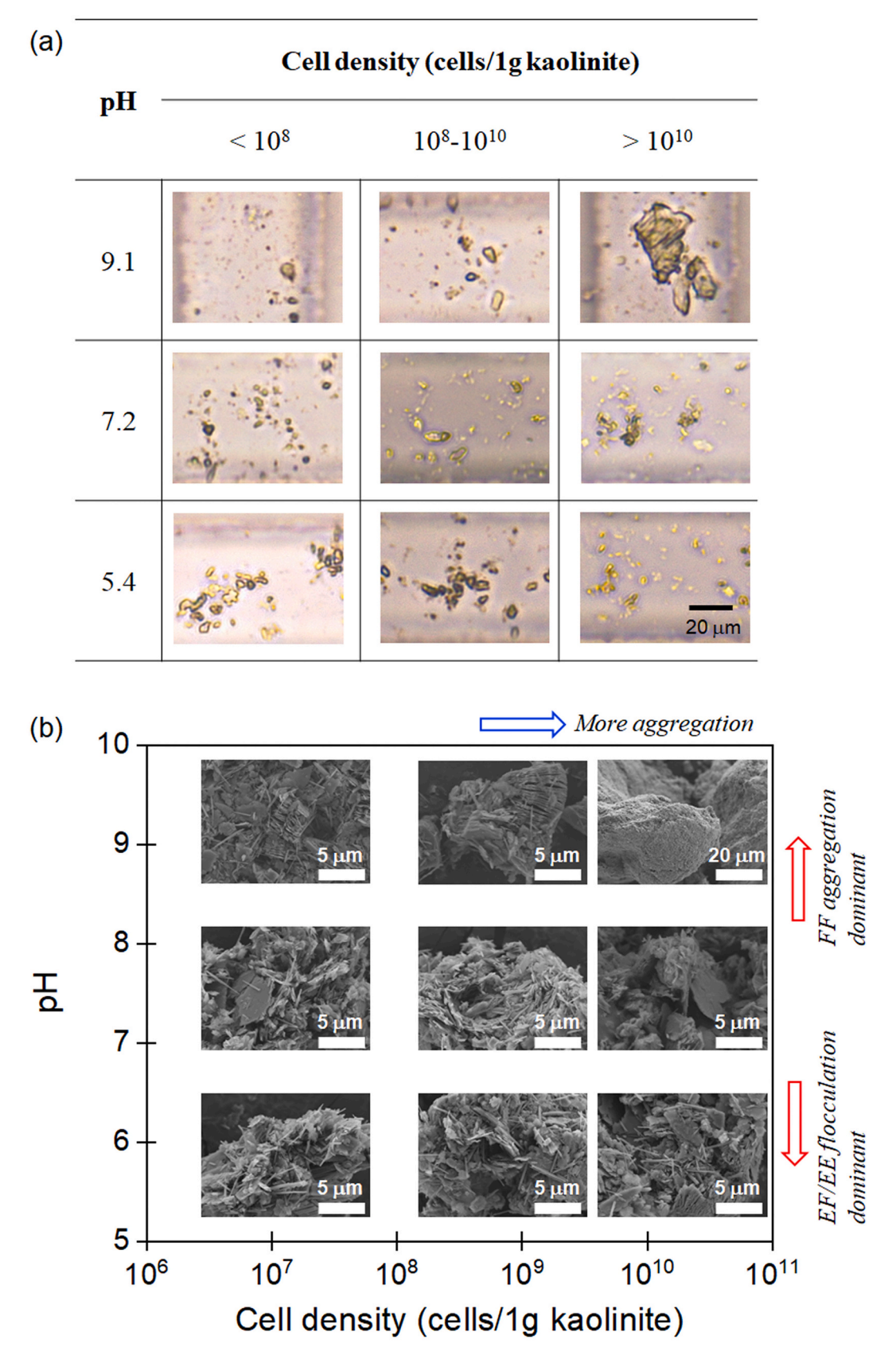
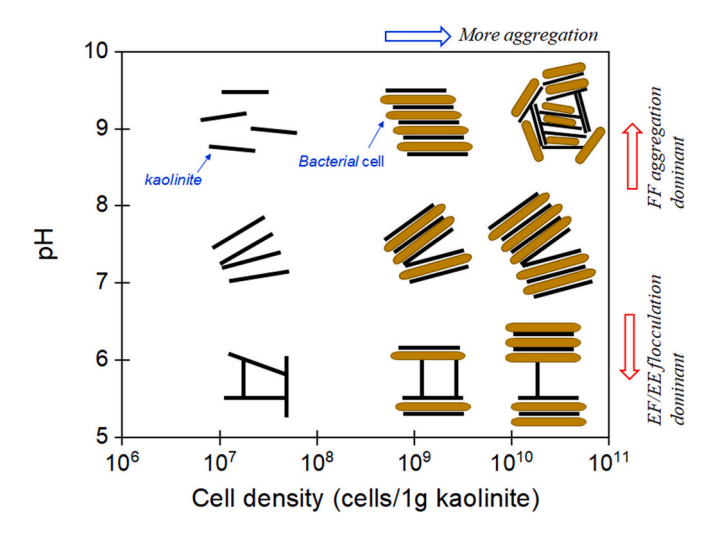


Fig. 11. Images of *S. oneidensis* MR-1 treated kaolinite clay: (a) optical images, (b) SEM images at various pH and cell density. The optical images are acquired on a microfluidic chip after diluting to 1.5 g/L kaolin suspensions, while maintaining the fluid chemistry and kaolinite-cell particle ratio constant.



**Fig. 12.** The fabric map of kaolinite clay in the presence of bacteria under a low salinity condition (*i.e.*, ~500 ppm in this study).

#### **Declaration of Competing Interest**

The authors declare that they have no known competing financial interests or personal relationships that could have appeared to influence the work reported in this paper.

#### Data availability

Data will be made available on request.

## Acknowledgements

The authors are grateful to Editor Pilar Aranda and two anonymous reviewers for their constructive comments and suggestions, which significantly improved the manuscript. This research was supported by the National Research Foundation of Korea (NRF) grant funded by the Korea government (MSIT) (No. NRF-2022R1A4A5031447), and S. Dai was financially supported by the National Science Foundation (CMMI-1943722).

#### Appendix A. Supplementary data

Supplementary data to this article can be found online at https://doi.org/10.1016/j.clay.2023.106973.

#### References

- Abboud, R., Popa, R., Souza-Egipsy, V., Giometti, C.S., Tollaksen, S., Mosher, J.J., Findlay, R.H., Nealson, K.H., 2005. Low-temperature growth of Shewanella oneidensis MR-1. Appl. Environ. Microbiol. 71, 811–816.
- Abu-Hassanein, Z.S., Benson, C.H., Blotz, L.R., 1996. Electrical resistivity of compacted clays. J. Geotech. Eng. 122, 397–406.
- Abu-Lail, N.I., Camesano, T.A., 2003. Role of ionic strength on the relationship of biopolymer conformation, DLVO contributions, and steric interactions to bioadhesion of *Pseudomonas putida* KT2442. Biomacromolecules 4, 1000–1012.
- Aiyama, K., Mizoguchi, K., Hirano, K., Takizawa, S., 2019. Effects of sample preparation on the microstructural signatures of faulting in clay-bearing fault gouge. J. Struct. Geol. 126, 100–108.
- Alimova, A., Katz, A., Steiner, N., Rudolph, E., Wei, H., Steiner, J.C., Gottlieb, P., 2009. Bacteria-clay interaction: structural changes in smectite induced during biofilm formation. Clay Clay Miner. 57, 205–212.
- Barhoum, A., García-Betancourt, M.L., Rahier, H., Van Assche, G., 2018. Physicochemical characterization of nanomaterials: polymorph, composition, wettability, and thermal stability. In: Emerging Applications of Nanoparticles and Architecture Nanostructures. Elsevier, pp. 255–278.
- Biswas, B., Chakraborty, A., Sarkar, B., Naidu, R., 2017. Structural changes in smectite due to interaction with a biosurfactant-producing bacterium *Pseudoxanthomonas kaohsiungensis*. Appl. Clay Sci. 136, 51–57.

- Brady, P.V., Walther, J.V., 1989. Controls on silicate dissolution rates in neutral and basic pH solutions at 25 C. Geochim. Cosmochim. Acta 53, 2823–2830.
- Castro-Smirnov, F.A., Pietrement, O., Aranda, P., Le Cam, E., Ruiz-Hitzky, E., Lopez, B.S., 2020. Biotechnological applications of the sepiolite interactions with bacteria: bacterial transformation and DNA extraction. Appl. Clay Sci. 191, 105613.
- Cen, L., Neoh, K., Kang, E., 2004. Antibacterial activity of cloth functionalized with N-alkylated poly (4-vinylpyridine). J. Biomed. Mater. Res. A: Off. J. Soc. Biomater. 71, 70–80. The Japanese Society for Biomaterials, and The Australian Society for Biomaterials and the Korean Society for Biomaterials.
- Chen, C., Pan, G., Shi, W., Xu, F., Techtmann, S.M., Pfiffner, S.M., Hazen, T.C., 2018. Clay flocculation effect on microbial community composition in water and sediment. Front. Environ. Sci. 6, 60.
- Chen, G., Pan, J., Han, B., Yan, H., 1999. Adsorption of methylene blue on montmorillonite. J. Dispers. Sci. Technol. 20, 1179–1187.
- Chen, L.-F., Liang, H.-W., Lu, Y., Cui, C.-H., Yu, Ś.-H., 2011. Synthesis of an attapulgite clay@ carbon nanocomposite adsorbent by a hydrothermal carbonization process and their application in the removal of toxic metal ions from water. Langmuir 27, 8998\_9004
- Chorom, M., Rengasamy, P., 1995. Dispersion and zeta potential of pure clays as related to net particle charge under varying pH, electrolyte concentration and cation type. Eur. J. Soil Sci. 46, 657–665.
- Danovaro, R., Corinaldesi, C., Filippini, M., Fischer, U.R., Gessner, M.O., Jacquet, S., Magagnini, M., Velimirov, B., 2008. Viriobenthos in freshwater and marine sediments: a review. Freshw. Biol. 53, 1186–1213.
- Derjaguin, B.V., Landau, L., 1941. Theory of the stability of strongly charged lyophobic sols and of the adhesion of strongly charged particles in solution of electrolytes. Acta Phys. Chim. USSR 14 (1–4), 633–662.
- Derjaguin, B.V., Churaev, N.V., Muller, V.M., 1987. Surface Forces. Springer Science & Business Media, New York.
- Dong, H., 2012. Clay–microbe interactions and implications for environmental mitigation. Elements 8, 113–118.
- Gadd, G.M., 2010. Metals, minerals and microbes: geomicrobiology and bioremediation. Microbiology 156, 609–643.
- Gorby, Y.A., Yanina, S., McLean, J.S., Rosso, K.M., Moyles, D., Dohnalkova, A., Beveridge, T.J., Chang, I.S., Kim, B.H., Kim, K.S., 2006. Electrically conductive bacterial nanowires produced by *Shewanella oneidensis* strain MR-1 and other microorganisms. Proc. Natl. Acad. Sci. U. S. A. 103, 11358–11363. Guo, Y.X., Liu, J.H., Gates, W.P., Zhou, C.H., 2020. Organo-modification of
- Guo, Y.X., Liu, J.H., Gates, W.P., Zhou, C.H., 2020. Organo-modification of montmorillonite. Clay Clay Miner. 68, 601–622.
- Hang, P.T., Brindley, G., 1970. Methylene blue absorption by clay minerals. Determination of surface areas and cation exchange capacities (clay-organic studies XVIII). Clay Clay Miner. 18, 203–212.
- Hasan, M.F., Abuel-Naga, H., Broadbridge, P., Leong, E.-C., 2018. Series-parallel structure-oriented electrical conductivity model of saturated clays. Appl. Clay Sci. 162, 239–251.
- Hassard, F., Gwyther, C.L., Farkas, K., Andrews, A., Jones, V., Cox, B., Brett, H., Jones, D. L., McDonald, J.E., Malham, S.K., 2016. Abundance and distribution of enteric bacteria and viruses in coastal and estuarine sediments—a review. Front. Microbiol. 7, 1692.
- Hayashi, H., Tsuneda, S., Hirata, A., Sasaki, H., 2001. Soft particle analysis of bacterial cells and its interpretation of cell adhesion behaviors in terms of DLVO theory. Colloids Surf. B: Biointerfaces 22, 149–157.
- Hogg, R., Healy, T.W., Fuerstenau, D.W., 1966. Mutual coagulation of colloidal dispersions. Trans. Faraday Soc. 62, 1638–1651.
- Hong, Z., Rong, X., Cai, P., Liang, W., Huang, Q., 2011. Effects of temperature, pH and salt concentrations on the adsorption of *Bacillus subtilis* on soil clay minerals investigated by microcalorimetry. Geomicrobiol J. 28, 686–691.
- Horie, M., Fujita, K., 2011. Toxicity of metal oxides nanoparticles. Adv. Mol. Toxicol. 145-178. Elsevier.
- Hunter, R.J., 2001. Foundations of Colloid Science, second ed. Oxford University Press, UK, pp. 581–637.
- Icopini, G.A., Lack, J.G., Hersman, L.E., Neu, M.P., Boukhalfa, H., 2009. Plutonium (V/VI) reduction by the metal-reducing bacteria Geobacter metallireducens GS-15 and Shewanella oneidensis MR-1. Appl. Environ. Microbiol. 75, 3641–3647.
- Imai, G., 1980. Settling behavior of clay suspension. Soils Found. 20, 61-77.
- Imai, G., 1981. Experimental studies on sedimentation mechanism and sediment formation of clay materials. Soils Found. 21, 7–20.
- Jia, C., Wei, D., Li, P., Li, X., Tai, P., Liu, W., Gong, Z., 2011. Selective adsorption of Mycobacterium Phlei on pyrite and sphalerite. Colloids Surf. B: Biointerfaces 83, 214-210
- Kim, Y.M., Kwon, T.H., 2022. Entrapment of clay particles enhances durability of bacterial biofilm-associated bioclogging in sand. Acta Geotech. 17, 119–129.
- Kumar, N., Andersson, M., Van den Ende, D., Mugele, F., Sîretanu, I., 2017. Probing the surface charge on the basal planes of kaolinite particles with high-resolution atomic force microscopy. Langmuir 33, 14226–14237.
- Kwon, Y.M., Im, J., Chang, I., Cho, G.C., 2017. ε-polylysine biopolymer for coagulation of clay suspensions. Geomech. Eng. 12, 753–770.
- Lavie, S., Stotzky, G., 1986. Adhesion of the clay minerals montmorillonite, kaolinite, and attapulgite reduces respiration of *Histoplasma capsulatum*. Appl. Environ. Microbiol. 51, 65–73.
- Lee, S., Kim, D.H., Kim, K.W., 2018. The enhancement and inhibition of mercury reduction by natural organic matter in the presence of *Shewanella oneidensis* MR-1. Chemosphere 194, 515–522.
- Leong, Y.K., Ong, B., 2003. Critical zeta potential and the Hamaker constant of oxides in water. Powder Technol. 134, 249–254.

- Li, G.L., Zhou, C.H., Fiore, S., Yu, W.H., 2019. Interactions between microorganisms and clay minerals: new insights and broader applications. Appl. Clay Sci. 177, 91–113.
- Ma, K., Pierre, A.C., 1992. Sedimentation behavior of a fine kaolinite in the presence of fresh Fe electrolyte. Clay Clay Miner. 40, 586–592.
- McMahon, S., Anderson, R.P., Saupe, E.E., Briggs, D.E., 2016. Experimental evidence that clay inhibits bacterial decomposers: implications for preservation of organic fossils. Geology 44, 867–870.
- Mhashhash, A., Bockelmann-Evans, B., Pan, S., 2018. Effect of hydrodynamics factors on sediment flocculation processes in estuaries. J. Soils Sediments 18, 3094–3103.
- Michaels, A.S., Bolger, J.C., 1962. Settling rates and sediment volumes of flocculated kaolin suspensions. Ind. Eng. Chem. Fundam. 1, 24–33.
- Missana, T., Adell, A., 2000. On the applicability of DLVO theory to the prediction of clay colloids stability. J. Colloid Interface Sci. 230, 150–156.
- Naimark, E., Eroshchev-Shak, V., Chizhikova, N., Kompantseva, E., 2009. Interaction of clay minerals with microorganisms: a review of experimental data. Zh. Obshch. Biol. 70, 155–167.
- Omoike, A., Chorover, J., 2006. Adsorption to goethite of extracellular polymeric substances from *Bacillus subtilis*. Geochim. Cosmochim. Acta 70, 827–838.
- Özcan, E., Selvi, S.S., Nikerel, E., Teusink, B., Toksoy Öner, E., Çakır, T., 2019. A genome-scale metabolic network of the aroma bacterium *Leuconostoc mesenteroides* subsp. cremoris. Appl. Microbiol. Biotechnol. 103, 3153–3165.
- Pachepsky, Y., Shelton, D., 2011. Escherichia coli and fecal coliforms in freshwater and estuarine sediments. Crit. Rev. Environ. Sci. Technol. 41, 1067–1110.
- Palomino, A.M., Santamarina, J.C., 2005. Fabric map for kaolinite: effects of pH and ionic concentration on behavior. Clay Clay Miner. 53, 211–223.
- Pan, G., Zhang, M.-M., Chen, H., Zou, H., Yan, H., 2006. Removal of cyanobacterial blooms in Taihu Lake using local soils. I. Equilibrium and kinetic screening on the flocculation of *Microcystis aeruginosa* using commercially available clays and minerals. Environ. Pollut. 141, 195–200.
- Parks, G.A., 1967. Aqueous Surface Chemistry of Oxides and Complex Oxide Minerals: Isoelectric Point and Zero Point of Charge. ACS Publications.
- Pashley, R., 1985. Electromobility of mica particles dispersed in aqueous solutions. Clay Clay Miner. 33, 193–199.
- Pecini, E.M., Avena, M.J., 2013. Measuring the isoelectric point of the edges of clay mineral particles: the case of montmorillonite. Langmuir 29, 14926–14934.
- Perdrial, J.N., Warr, L.N., Perdrial, N., Lett, M.-C., Elsass, F., 2009. Interaction between smectite and bacteria: implications for bentonite as backfill material in the disposal of nuclear waste. Chem. Geol. 264, 281–294.
- Pierre, A., Ma, K., Barker, C., 1995. Structure of kaolinite flocs formed in an aqueous medium. J. Mater. Sci. 30, 2176–2181.
- Qu, C., Ma, M., Chen, W., Cai, P., Huang, Q., 2017. Surface complexation modeling of Cu (II) sorption to montmorillonite–bacteria composites. Sci. Total Environ. 607, 1408–1418.
- Ray, R., Lizewski, S., Fitzgerald, L., Little, B., Ringeisen, B., 2010. Methods for imaging Shewanella oneidensis MR-1 nanofilaments. J. Microbiol. Methods 82, 187–191.
- Revil, A., Atekwana, E., Zhang, C., Jardani, A., Smith, S., 2012. A new model for the spectral induced polarization signature of bacterial growth in porous media. Water Resour. Res. 48.
- Roy, J.N., Garcia, K.E., Luckarift, H.R., Falase, A., Cornejo, J., Babanova, S., Schuler, A. J., Johnson, G.R., Atanassov, P.B., 2013. Applied electrode potential leads to Shewanella oneidensis MR-1 biofilms engaged in direct electron transfer. J. Electrochem. Soc. 160, H866.
- Santamarina, J.C., Klein, K.A., Palomino, A., Guimaraes, M.S., 2002a. Micro-scale aspects of chemical-mechanical coupling: interparticle forces and fabric. In: Chemical Behaviour: Chemo-Mechanical Coupling from Nano-Structure to Engineering Applications, pp. 47–64.
- Santamarina, J.C., Klein, K.A., Wang, Y.H., Prencke, E., 2002b. Specific surface: determination and relevance. Can. Geotech. J. 39, 233–241.

- Sapsford, K.E., Tyner, K.M., Dair, B.J., Deschamps, J.R., Medintz, I.L., 2011. Analyzing nanomaterial bioconjugates: a review of current and emerging purification and characterization techniques. Anal. Chem. 83, 4453–4488.
- Scales, P.J., Johnson, S.B., Healy, T.W., Kapur, P.C., 1998. Shear yield stress of partially flocculated colloidal suspensions. AICHE J. 44, 538–544.
- Schofield, R., Samson, H., 1954. Flocculation of kaolinite due to the attraction of oppositely charged crystal faces. Discuss. Faraday Soc. 18, 135–145.
- Shnoudeh, A.J., Hamad, I., Abdo, R.W., Qadumii, L., Jaber, A.Y., Surchi, H.S., Alkelany, S.Z., 2019. Synthesis, characterization, and applications of metal nanoparticles. In: Biomaterials and Bionanotechnology. Elsevier, pp. 527–612.
- Su, M., Han, F., Wu, Y., Yan, Z., Lv, Z., Tian, D., Wang, S., Hu, S., Shen, Z., Li, Z., 2019. Effects of phosphate-solubilizing bacteria on phosphorous release and sorption on montmorillonite. Appl. Clay Sci. 181, 105227.
- Syngouna, V.I., Chrysikopoulos, C.V., 2010. Interaction between viruses and clays in static and dynamic batch systems. Environ. Sci. Technol. 44, 4539–4544.
- Tombácz, E., Szekeres, M., 2006. Surface charge heterogeneity of kaolinite in aqueous suspension in comparison with montmorillonite. Appl. Clay Sci. 34, 105–124.
- Tournassat, C., Bourg, I.C., Steefel, C.I., Bergaya, F., 2015. Surface properties of clay minerals. In: Developments in Clay Science. Elsevier, pp. 5–31.
- Tsujimoto, Y., Chassagne, C., Adachi, Y., 2013. Comparison between the electrokinetic properties of kaolinite and montmorillonite suspensions at different volume fractions. J. Colloid Interface Sci. 407, 109–115.
- van Olphen, H., 1964. An introduction to clay colloid chemistry. Soil Sci. 97, 290. van Olphen, H., 1977. An Introduction to Clay Colloid Chemistry: For Clay
- van Olphen, H., 1977. An Introduction to Clay Colloid Chemistry: For Clay Technologists, Geologists, and Soil Scientists, second ed. John Wiley & Sons, New York, pp. 92–110.
- Verwey, E.J.W., 1947. Theory of the stability of lyophobic colloids. J. Phys. Chem. 51, 631–636.
- Wieland, E., Stumm, W., 1992. Dissolution kinetics of kaolinite in acidic aqueous solutions at 25 C. Geochim. Cosmochim. Acta 56, 3339–3355.
- Williams, D., Williams, K., 1978. Electrophoresis and zeta potential of kaolinite. J. Colloid Interface Sci. 65, 79–87.
- Wilson, L.A., Butterfield, N.J., 2014. Sediment effects on the preservation of Burgess Shale-type compression fossils. Palaios 29, 145–154.
- Xiong, Y., Shi, L., Chen, B., Mayer, M.U., Lower, B.H., Londer, Y., Bose, S., Hochella, M. F., Fredrickson, J.K., Squier, T.C., 2006. High-affinity binding and direct electron transfer to solid metals by the *Shewanella oneidensis* MR-1 outer membrane c-type cytochrome OmcA. J. Am. Chem. Soc. 128, 13978–13979.
- Yee, N., Fein, J.B., Daughney, C.J., 2000. Experimental study of the pH, ionic strength, and reversibility behavior of bacteria–mineral adsorption. Geochim. Cosmochim. Acta 64, 609–617.
- Yong, R.N., Ohtsubo, M., 1987. Interparticle action and rheology of kaolinite-amorphous iron hydroxide (ferrihydrite) complexes. Appl. Clay Sci. 2, 63–81.
- Zhang, T., Yang, W., Zhu, X., Wang, H., Brookes, P.C., Xu, J., 2015. The pH dependence of Escherichia coli O157: H7 adsorption on kaolinite and goethite surfaces. J. Soils Sediments 15, 106–116.
- Zhang, Y., Wang, F., Tian, Q., Shen, Z., 2022. Natural or engineered clays for stabilization/solidification. In: Low Carbon Stabilization and Solidification of Hazardous Wastes. Elsevier, pp. 31–47.
- Zhou, C.H., Keeling, J., 2013. Fundamental and applied research on clay minerals: from climate and environment to nanotechnology. Appl. Clay Sci. 74, 3–9.
- Zhou, C.H., Zhao, L.Z., Wang, A.Q., Chen, T.H., He, H.P., 2016. Current fundamental and applied research into clay minerals in China. Appl. Clay Sci. 119, 3–7.
- Zou, H., Pan, G., Chen, H., Yuan, X., 2006. Removal of cyanobacterial blooms in Taihu Lake using local soils II. Effective removal of *Microcystis aeruginosa* using local soils and sediments modified by chitosan. Environ. Pollut. 141, 201–205.